Simulation of a Structurally-Controlled Gold Deposit using High-Order Statistics

David F. Machuca-Mory[1] and Roussos Dimitrakopoulos[2]

Abstract The algorithm for conditional simulation based on spatial high-order statistics is applied to a drilling dataset obtained from a structurally complex gold deposit, the Apensu deposit in Ghana. Spatial high-order statistics allow capturing nonlinear spatial features of the gold mineralization that variograms and covariances cannot. Since robust spatial high-order statistics cannot be inferred only from scattered samples, they are borrowed from a training image. In this case, sequential Gaussian simulation with local variograms within domain boundaries is used to build a training image. At different locations HOSIM uses the spatial high-order statistics to approximate non-Gaussian distributions of possible values conditioned by neighboring data. The effect of sampling clustering in the probability distribution and its statistics is taken into account by incorporating declustering weights in the inference of low and high-order statistics required by high-order simulation. The resulting realizations reproduce the cdf and the low-order statistics of data and tend to approach the high order statistics of the training image. They also reproduce the gold-rich major and well sampled structures. The reproduction of small structures and undersampled is hindered by the use of a Gaussian based training image and the similitude of their gold grade populations to those of the background host rock.

Introduction

Structural processes, such as faulting and folding, are often the major controls of the spatial distribution of grades in diverse deposits. Grades are higher within and in the proximity of faults that act as mineralization feeders and tend to fade away from them. Moreover, mineralized rock layers are often bended and discontinuous. The resulting structural setting of a deposit is often complex and it is seldom fully mapped, whereas measurements of grades are limited in number.

[1] Stochastic Mine Planning Laboratory COSMO, Department of Mining and Materials Engineering, McGill University, 3450 University St. Rm 123A, Montreal, QC Canada, david.machucamory@mcgill.ca

[2] Stochastic Mine Planning Laboratory COSMO, Department of Mining and Materials Engineering, McGill University, 3450 University St. Rm 123A, Montreal, QC Canada, roussos.dimitrakopoulos@mcgill.ca

This calls for the characterization of the grade distribution uncertainty in mineral resources models. A common approach is to describe the range of possible scenarios by the ensemble multiple realizations generated using Sequential Gaussian Simulation (SGS). However, besides the linear spatial continuity imposed by the variogram model, SGS realizations show the characteristic maximum entropy pattern [1] resulting from the adoption of the Gaussian model for the distribution of continuous values. In certain cases, different patterns of the spatial distribution of grades can be associated to different geological units. In such cases, the common practice is to use categorical simulation techniques for the modeling of the geological units in combination with SGS for the modeling of grades within the units. Among the commonly used techniques for the modeling of categorical variables for mining applications are Sequential Indicator Simulation [2], Plurigaussian Simulation [3] and simulation based on multiple point statistics [4-6]. Proceeding in this way allows introducing complex spatial features in the simulated models.

This paper presents the algorithm of simulation based on spatial high-order statistics, or High-Order Simulation (HOSIM) [7, 8] as an alternative to the combined approach for the modeling of grades. Spatial high-order statistics, such as moments and cumulants, are able to capture non-linear and high-order spatial features from data and training images [9, 10]. At each location in a grid, HOSIM uses these high-order statistics to approximate the local non-Gaussian distributions conditioned by neighboring data values. The resulting realizations reproduce not only the histogram and covariance of the original data, but also the high-order statistics of data and the training image. The next section contains an overview of the theory of spatial high-order statistics and their use for fitting non-Gaussian multivariate conditional distributions in a sequential simulation framework. Weighted high-order moments are presented as a way to account for data clustering when inferring the non-Gaussian conditional distributions. A dataset consisting of drill-hole samples and a geological model is used to build a continuous training image. HOSIM integrates the samples and the training image for the inference of high-order statistics. Using this initial information, multiple HOSIM realizations are generated. The capability of HOSIM realizations to reproduce the low and high-order statistics of the initial information, which is a validity test for any geostatistical simulation method [11], is assessed. The last part of this paper discusses the potential and current limitations of this new simulation approach and the undergoing work aimed to improve this algorithm.

Simulation Based on High-Order Statistics

This section provides a brief introduction to high-order spatial statistics and their use for approximating multivariate non-Gaussian distributions. The HOSIM

algorithm is presented as an implementation of this theory for the simulation of non-Gaussian variables in a sequential framework.

High-Order Spatial Statistics

Consider a spatial random function $Z(\mathbf{u})$ defined over a domain D and $\mathbf{u}$ as a location within that domain. The vectors $\mathbf{h}_1, \cdots, \mathbf{h}_n$ define a template $T_{n+1}^{\mathbf{h}_1,\ldots,\mathbf{h}_n}$ of $n+1$ points $\mathbf{u}_0, \mathbf{u}_0+\mathbf{h}_1, \ldots, \mathbf{u}_0+\mathbf{h}_n$. The set of set random variables corresponding to the points in the template are $Z(\mathbf{u}_o) = Z_0$, $Z(\mathbf{u}_o+\mathbf{h}_1) = Z_1, \cdots Z(\mathbf{u}_o+\mathbf{h}_n) = Z_n$, A high-order spatial moment for this arrangement is defined by the integration

$$E\left[Z_0^{i_0} \cdot Z_1^{i_1} \cdots Z_n^{i_n}\right] = \int_{D^{n+1}} z_o^{i_0} z_1^{i_1} \cdots z_n^{i_n} f_{\mathbf{Z}}(z_0 z_1 \cdots z_n) d\mathbf{z}, \quad (1)$$

with $\mathbf{z} = (z_0, z_{1,} \cdots, z_n)$. The experimental high-order spatial moments are obtained by the average of the product of the values $z_0, z_{1,} \cdots, z_n$ for all instances where the arrangement of sample locations defined by $\mathbf{u}_o, \mathbf{u}_o+\mathbf{h}_1, \cdots, \mathbf{u}_o+\mathbf{h}_n$ is replicated. Sampling of mineral deposits often is clustered in the richest areas. This results in biased grades distributions and statistics. Spatial declustering methods are used to assign higher weights to isolated samples and lower weights to samples in densely samples areas. These weights are incorporated in the estimation of declustered distributions and its statistics. Following this idea, declustered high-order moments can be inferring by incorporating multiple-point declustering weights. The proposed form of multiple-point declustering weights is obtained by the geometrical average of the individual declustering weights, $w_i, i = 0, \ldots, n$ assigned to each sample in a template $T_{n+1}^{\mathbf{h}_1,\ldots,\mathbf{h}_n}$:

$$w_{\mathbf{u}_0,1,\ldots,n} = w[z_0, z_1, \cdots, z_n] = \sqrt[n+1]{w_0 w_1 \cdots w_n}. \quad (2)$$

If the template $T_{n+1}^{\mathbf{h}_1,\ldots,\mathbf{h}_n}$ has $N_{h_1 \cdots h_n}$ replicates within the domain, the corresponding weighted experimental high-order moment can be inferred by

$$\hat{E}^{(w)}\left[Z_0^{i_0} Z_1^{i_1} \cdots Z_n^{i_n}\right] = \frac{1}{\sum_k^{N_{h_1 \cdots h_n}} w_{\mathbf{u}_k,1,\ldots,n}} \sum_{j=1}^{N_{h_1 \cdots h_n}} w_{\mathbf{u}_j,1,\ldots,n} z_j^{i_0} z_1^{i_1} \cdots z_n^{i_n}. \quad (3)$$

Moments can be expressed as combinations of cumulants of the same and lower order, and viceversa [12]. For a zero-mean random function, the spatial cumulants from order one to four are given by

$$
\begin{aligned}
C_1(Z_0) &= E[Z_0] = 0,\\
C_2(Z_0, Z_1) &= C_2(\mathbf{h}_1) = E[Z_0 Z_1],\\
C_3(Z_0, Z_1, Z_2) &= C_3(\mathbf{h}_1, \mathbf{h}_2) = E[Z_0 Z_1 Z_2],\\
C_4(Z_0, Z_1, Z_2, Z_3) &= C_3(\mathbf{h}_1, \mathbf{h}_2, \mathbf{h}_3) = E[Z_0 Z_1 Z_2 Z_3] - \\
&\quad E[Z_0 Z_1]E[Z_2 Z_3] - E[Z_0 Z_2]E[Z_1 Z_3] - \\
&\quad E[Z_0 Z_3]E[Z_1 Z_2].
\end{aligned}
\tag{4}
$$

Note that the first cumulant is the mean and the second is the spatial covariance. Thus, spatial cumulants can be understood as the multiple-point generalization of the covariance.

Approximation of a Non-Gaussian Multivariate pdf

In conditional simulation, the distribution of values at any unsampled location is conditioned by the input information, particularly a dataset $d_n = \{z(\mathbf{u}_\alpha) = z_\alpha, \alpha = 1, \dots, n\}$, and previously simulated nodes. If the initial conditioning data is $\Delta_0 = \{d_n\}$, the conditional pdf at a location $\mathbf{u}_0$ is given by

$$
\mathrm{f}_{\mathrm{Z}_0}(\mathrm{z}_\mathrm{o}|\Delta_0) = \frac{\mathrm{f}_\mathrm{Z}(\mathrm{z}_0, \mathrm{z}_1, \dots, \mathrm{z}_\mathrm{n})}{\int_\mathrm{A} \mathrm{f}_\mathrm{Z}(\mathrm{z}_0, \mathrm{z}_1, \dots, \mathrm{z}_\mathrm{n})\mathrm{dz}_0}. \tag{5}
$$

With A as the domain where $f_Z$is defined. Once the conditional pdf is built, a realization is subsequently drawn from it. This newly simulated value, z'_0 is added to the dataset. Thus, the new conditioning data consists of $\Delta_1 = \{d_n\} \cup \{z'_0\}$ and is used to condition the pdf at a second node. This process continues by following a random path until all nodes of the predefined grid are simulated [13] .

The main problem is to infer the multivariate distribution in the numerator of expression (5). In Sequential Gaussian Simulation, for instance, the multivariate pdf is efficiently modeled by a multiGaussian distribution, which is fully defined by a covariance matrix and a vector of local means. In a different fashion, high-order simulation uses high-order statistics and Legendre polynomials. For example, consider an unsampled location $\mathbf{u}_0$ and two conditioning data, z_1 and z_2, the corresponding declustered multivariate pdf is given by [14]

$$
f_Z^{(w)}(z_o, z_1, z_2) = \frac{w(z_o, z_1, z_2) f_Z(z_o, z_1, z_2)}{E[w(z_o, z_1, z_2)]}. \tag{6}
$$

If the marginal pdfs are defined in $A = [-1,1]$, which usually requires rescaling the original values, the multivariate pdf can be expressed as a series of Legendre polynomials [7]:

$$f_Z^{(w)}(z_o, z_1, z_2) = \sum_{l=0}^{\infty}\sum_{m=0}^{\infty}\sum_{n=0}^{\infty} L_{l,m,n}^{(w)} \bar{P}_l(z_0)\bar{P}_m(z_1)\bar{P}_n(z_2). \quad (7)$$

$L_{l,m,n}^{(w)}$ are the weighted Legendre coefficients and $\bar{P}_\alpha(z), \alpha = l, m, n$, are the α-order normalized Legendre polynomials, such as:

$$\bar{P}_\alpha(z) = \sqrt{\frac{2\alpha+1}{2}} P_\alpha(z). \quad (8)$$

The first two Legendre polynomials are $P_0(z) = 1$ and $P_1(z) = z$. The following derivation allows obtaining Legendre polynomials of any order $\alpha \geq 0$,

$$P_\alpha(z) = \frac{1}{2^\alpha \alpha!}\frac{d^\alpha}{dz^\alpha}[(z^2-1)^\alpha] = \sum_{j=1}^{\alpha} a_{j,\alpha} z^\alpha, \text{for } z \in [-1,1]. \quad (9)$$

The Legendre polynomials fulfill the orthogonally property. If they are normalized this property is defined as

$$\int_A \bar{P}_m(z)\bar{P}_n(z)dz = \begin{cases} 0, \text{if } m \neq n \\ 1, \text{if } m = n. \end{cases} \quad (10)$$

After applying this property on Equation (7), the Legendre coefficients are derived as

$$L_{l,m,n}^{(w)} = \int_{A^3} \bar{P}_l(z_0)\bar{P}_m(z_1)\bar{P}_n(z_2) f_Z^{(w)}(z_o, z_1, z_2) dz_0 dz_1 dz_2. \quad (11)$$

Doing $\bar{a}_{i,\alpha} = a_{i,\alpha}\sqrt{(2\alpha+1)/2}$ and recurring to Equation (9), the Legendre coefficients above become

$$L_{l,m,n}^{(w)} = \sum_{i=0}^{l}\sum_{j=0}^{m}\sum_{k=0}^{n} \bar{a}_{i,l}\,\bar{a}_{j,m}\bar{a}_{k,n} \int_{A^3} z_0^i z_1^j z_2^k f_Z^{(w)}(z_o, z_1, z_2) dz_0 dz_1 dz_2. \quad (12)$$

Therefore, these coefficients can be expressed as combinations of the weighted high-order moments:

$$L_{l,m,n}^{(w)} = \sum_{i=0}^{l}\sum_{j=0}^{m}\sum_{k=0}^{n} \bar{a}_{i,l}\,\bar{a}_{j,m}\bar{a}_{k,n} E^{(w)}\left[Z_0^i Z_1^j Z_2^k\right]. \quad (13)$$

Fitting a multivariate non-Gaussian distribution in this way can be computationally demanding. For this reason, the expansion of the Legendre polynomial series in (7) is truncated to an order ω, which is not larger than 10, as a rule of thumb. Therefore, approximation of the multivariate pdf becomes

$$f_Z^{(w)}(z_o, z_1, z_2) = \sum_{l=0}^{\omega} \sum_{m=0}^{l} \sum_{n=0}^{m} L_{l,m,n}^{(w)} \bar{P}_l(z_0) \bar{P}_m(z_1) \bar{P}_n(z_2). \quad (14)$$

When the moments involve one to two points, they can be inferred directly from available samples. However, as the number of points in the high-order moment template increases, the replicates required for the robust inference of these moments become scarcer. For this reason, a training image deemed representative of the spatial distribution of grades is used to provide the required high-order spatial statistics. The HOSIM algorithm scans the samples and training image to obtain and store all the required high-order statistics that fall within a search volume. Subsequently, HOSIM proceeds to the inference of the conditional pdf at the nodes of a grid. The high-order statistics that correspond to the spatial template defined by the neighbouring samples to a node is retrieved from the storage and used to approximate the conditional pdf. The following section illustrates the application of this new simulation algorithm to the data obtained from a structurally controlled gold deposit.

Application to a Structurally Controlled Gold Deposit

The dataset used for illustrating the application of HOSIM is a subset of a larger drilling campaign dataset from the Apensu deposit, located in the Ahafo South district of Ghana and owned by Newmont Ghana Gold Ltd. The gold mineralization in this deposit is controlled by the dominant thrust fault and its subsidiary structures. The richer gold grades are found mainly in the hanging wall of the thrust fault [6]. Newmont provided the drilling dataset containing the gold assays, as well as a tridimensional geological model of the thrust fault and the two families of subsidiary structures. Taking into account the host rock, this model defines four mineralization domains.

Original Data and Training Image

The selected region for this study comprises a volume of $300m \times 600m \times 150m$, which was rotated to make the fault thrust strike parallel to the North South direction. This region is located at the center of the deposit, which is the most densely sampled area. Figure 1(a) shows a 3D view of the mineralization domains in the selected region. Figure 1(b) shows the drill-hole traces in the selected region. Drill-holes are, for the most part, perpendicular or sub-perpendicular to the mail fault thrust.

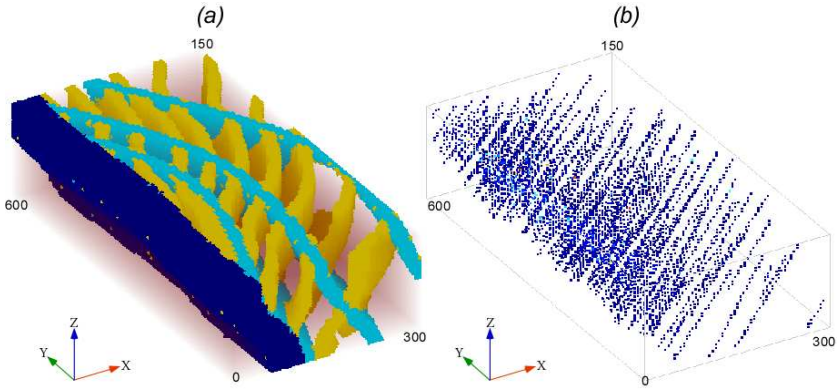

Figure 1 (a) Geological model view showing the main fault zone (dark blue) and the two families of subsidiary structures (pale blue and golden). (b) A similar view showing the drill-hole traces

The samples within the selected region were composited in 5m intervals and the composited gold grades rescaled between 0 and 10. This last was done for confidentiality reasons. The cell declustering method [13] was used to assign declustering weights to the composites. Table 1 shows the basic statistics for the clustered and declustered 4106 composited in the selected region. As this table shows, the impact of data clustering in the Au cdf and its statistics is significant.

Table 1: Basic statistics for clustered and declustered Gold composites

Statistics for (Au $g/(t \times 10)$) :	Mean	Std. Dev.	Q25	Q50	Q75
Clustered composites:	0.24	0.52	0.03	0.09	0.22
Declustered composites:	0.19	0.44	0.02	0.06	0.16

Figure 2(a) shows the cumulative probabilities of composites grouped by domains. The richer gold population is present in the fault thrust domain, whereas the distribution of gold grades in the other three domains, the subsidiary structures and the host rock, are very similar among them. As Figure 2(b) shows, the host rock contains most of the composites, followed by the fault domain. Only 13% of the total number of composites belongs to the two families of subsidiary structures. This and the fact that the grades distributions in the subsidiary structures are similar to the grades distribution in the host rock, make it difficult to characterize their corresponding mineralization spatial patterns.

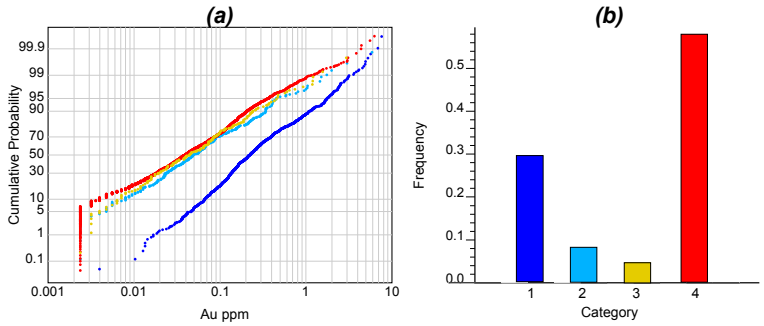

Figure 2 (a) Cumulative probabilities of gold grades and (b) proportion of samples in the fault zone (blue), subsidiary structures (pale blue and golden) and host rock (red)

The required training image was built using sequential Gaussian simulation (SGS) with location-dependent variograms [15] that follow the geometry of the domains. The domain boundaries were defined as hard, this is only composites within the boundaries of a domain were used for simulating the grades in it. The dimensions of the training image are the same as the dimensions of the zone of study. It is important to remark that the use of SGS for the construction of the training image raises concerns about its ability to reproduce the high-order statistics of data, given that the high-order cumulants of Gaussian distributions tend to zero [16]. However, there are few practical alternatives to SGS within domains for the construction of training images from scattered samples.

Figure 3 shows the third order (at the left) and fourth order (at the right) cumulants obtained from the composites (at the top) and the training image (at the bottom). These cumulants were calculated using tridimensional templates formed by vectors $\mathbf{h}_X, \mathbf{h}_Y$ and $\mathbf{h}_Z$ of different lengths and parallel to the X, Y and Z axes, respectively. Despite its patchiness, the third and fourth order cumulant maps of composites (Figure 3(a) and Figure 3(b), respectively) show a higher continuity along the Y axis. This is clearly related to the continuity of high grades in the fault domain. The fluctuations of the cumulants in the direction parallel to the X and Z axes are related to the interaction of high grades in the fault domain and the subsidiary structures at the east.

The third and fourth order cumulant maps of the training image (Figure 3(c) and Figure 3(d), respectively) show features comparable to the cumulant maps of composites, but the former appear more continuous. This is because there is no lack of replicates for the templates used to calculate the cumulants but also because the use of SGS in the construction of the training image.

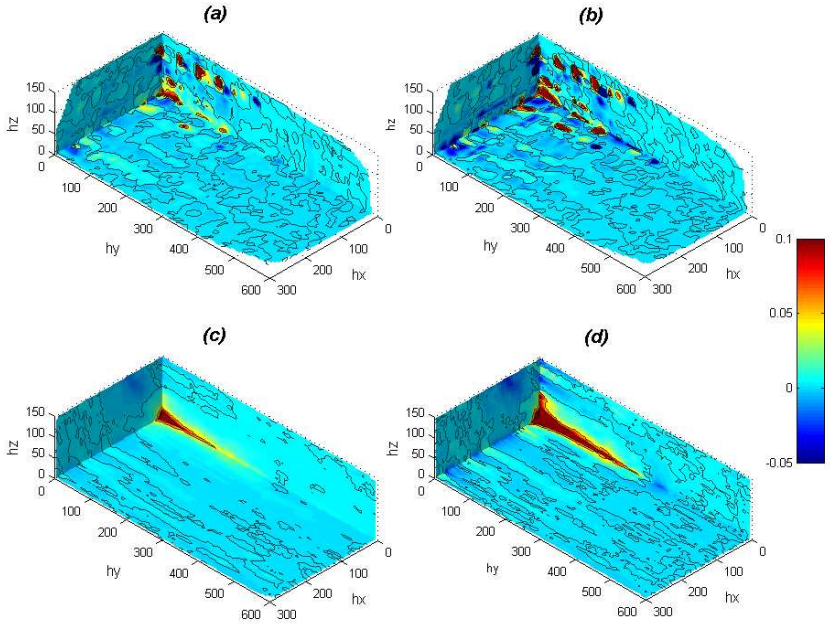

Figure 3 (a) and (b): third and fourth order, respectively, cumulant maps for the composited samples. (c) and (d): third and fourth order, respectively, cumulant maps for the training image.

High-Order Simulation

The composite dataset and the training image described in the previous section were used as inputs for the HOSIM algorithm. HOSIM superimposes the data to the training image and rescales the merged values between 0 and 1. Before simulating the grades, HOSIM scans the merged training to obtain and store the high-order statistics for all the spatial templates that can be accommodated in a search template. In this case, the dimensions of the search template were 75m x 135m x 55m, with the longer side parallel to the *y* axis. The declustering sample weights were also superimposed to the equal weights of the training image nodes. The maximum number of neighboring samples to condition the simulation of a node was set as 24, and the order of the polynomial series was 7. A larger number of samples or higher orders for the Legendre polynomials increase considerably the computational effort with modest improvement of the realizations. Twenty HOSIM realizations were generated; Figure 4(b) shows a 3D sectional view of a

randomly chosen HOSIM realization. Figure 4(a) shows a similar view for the training image.

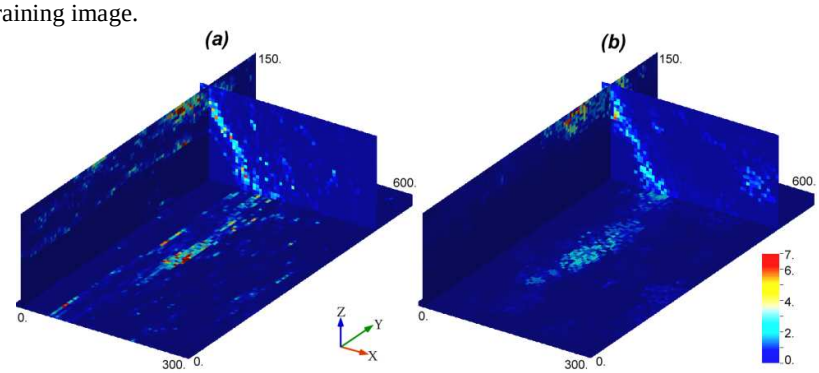

Figure 4 Sectional views of the training image (a) and a randomly chosen HOSIM realization (b)

HOSIM realizations reproduce the high grade mineralization of the fault domain without need of constraining the simulation within domain boundaries, as in the case of SGS realizations. However, the mineralization in the subsidiary structures is poorly reproduced in the HOSIM realizations, but this also happens in the training image. As Figure 5 shows, HOSIM realizations using weighted high-order statistics reproduce the declustered cumulative probability distribution of original data. The reproduction of the data covariance in different directions is also acceptable (see Figure 6). The third and fourth order cumulants maps of the realizations are smoother than similar cumulant maps obtained from data.

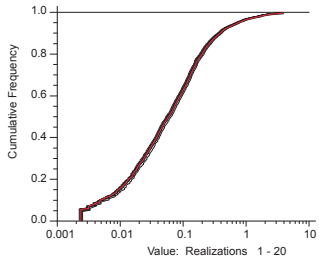

Figure 5 Cumulative probability distributions of composite data (red line) and HOSIM realizations (black lines)

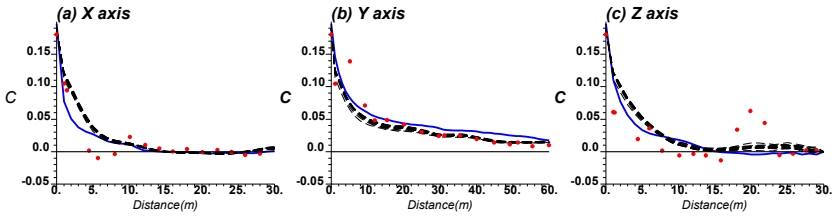

Figure 6 Covariances of composite data (red dots), training image (solid blue line) and HOSIM realizations (dashed black line) in the directions parallel to the X axis (a), Y axis (b) and Z axis (c)

The cumulant maps of HOSIM realizations tend to approach those obtained from the training image as the order of the cumulants increases. However, as it can be observed in Figure 7, some features present in the cumulant maps of declustered data are also reproduced in the third and fourth order cumulant maps of a HOSIM realization. These features include a shorter continuity along the Y axis than shown by the training image cumulant maps, and the eastward fluctuations of the realization's cumulant values, which are higher than those shown in similar maps corresponding to the training image.

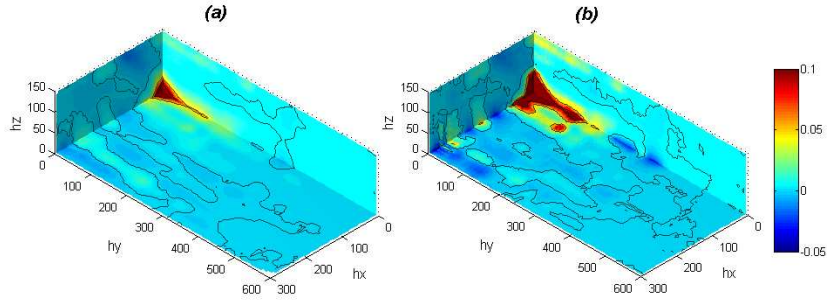

Figure 7 third order (a) and fourth order (b) cumulant maps of the HOSIM realization shown in Figure 4(b)

Discussion and Conclusions

The incorporation of declustering weights in the inference of the low and high-order statistics allows HOSIM to reproduce the declustered data cdf and its low order statistics. Differently from widespread simulation techniques, such as sequential Gaussian simulation, HOSIM can also produce realizations that contain the high-order statistics of the data and the training image.

The higher the order of the statistics the closer the realizations statistics will approach those of the training image. This is expected, since only an exhaustive image can provide enough replicates needed to infer the high-order statistics. This poses the problem of availability of training images that are rich in high-order spatial structures. For the case study presented in this paper, the training image was built using sequential Gaussian simulation within boundaries and using local variograms. This methodology introduces more complex spatial structures in the training image, but its high-order statistics still tend to zero quicker than those of the dataset. The generation of non-Gaussian continuous training images containing low and high-order statistics representative of the phenomenon to be simulated is a subject of ongoing research.

HOSIM realizations are able to reproduce the main spatial features of the mineralization without being constrained by domain boundaries. In the case presented, the spatial distribution and values of the high grade mineralization in the fault domain are honored in the realizations. The mineralization patterns in the subsidiary structures, however, are more difficult to reproduce. This is due to the low number of samples taken within these structures, and the similitude of their corresponding cdfs with the cdfs of gold grades in the host rock. A related subject of future research is the incorporation of weights obtained from the Tau model [17]. This may allow reducing the impact of background noisy information in the inference of the high-order statistics and the conditional pdfs, and thus enhancing the reproduction of the spatial features related to the mineralization controls.

Acknowledgements

This work was funded from NSERC CDR Grant 335696 and BHP Biliton, as well NSERC Discovery Grant 239019, and the Cosmo Consortium. Thanks are in order to Brian Baird, Peter Stone, Gavin Yates and Darren Dyck, for their support and collaboration, as well as to Newmont's Ian Douglas, Larry Allen, and Arja Jewbali for providing the data used herein, as well as for support, comments and assistance in understanding the Apensu deposit

Bibliography

[1] A. Journel and C. Deutsch, "Entropy and spatial disorder," *Mathematical Geology*, vol. 25, pp. 329-355, 1993.

[2] R. Srivastava, "Probabilistic Modeling of Ore Lens Geometry: An Alternative to Deterministic Wireframes," *Mathematical Geology*, vol. 37, pp. 513-544, 2005.

[3] M. Armstrong, A. G. Galli, H. Beucher, G. Le Loc'h, D. Renard, B. Doligez, R. Eschard, and F. Geffroy, *Plurigaussian Simulations in Geosciences*: Springer, 2011.

[4] S. Strebelle, "Conditional Simulation of Complex Geological Structures Using Multiple-Point Statistics," *Mathematical Geology,* vol. 34, pp. 1-21, 2002.

[5] R. Goodfellow, F. Albor Consuegra, R. Dimitrakopoulos, and T. Lloyd, "Quantifying multi-element and volumetric uncertainty, Coleman McCreedy deposit, Ontario, Canada," *Computers & Geosciences,* vol. 42, pp. 71-78, 2012.

[6] P. Jones, I. Douglas, and A. Jewbali, "Modelling geological uncertainty in mining using multiple-point statistics," in *World Gold 2011, 3rd International Conference*, Montreal QC, 2011.

[7] H. Mustapha and R. Dimitrakopoulos, "High-order Stochastic Simulation of Complex Spatially Distributed Natural Phenomena," *Mathematical Geosciences,* vol. 42, pp. 457-485, 2010.

[8] H. Mustapha and R. Dimitrakopoulos, "HOSIM: A high-order stochastic simulation algorithm for generating three-dimensional complex geological patterns," *Computers & Geosciences,* vol. 37, pp. 1242-1253, 2011.

[9] R. Dimitrakopoulos, H. Mustapha, and E. Gloaguen, "High-order Statistics of Spatial Random Fields: Exploring Spatial Cumulants for Modeling Complex Non-Gaussian and Non-linear Phenomena," *Mathematical Geosciences,* vol. 42, pp. 65-99, 2010.

[10] H. Mustapha and R. Dimitrakopoulos, "A new approach for geological pattern recognition using high-order spatial cumulants," *Computers & Geosciences,* vol. 36, pp. 313-334, 2010.

[11] O. Leuangthong, J. A. McLennan, and C. V. Deutsch, "Minimum Acceptance Criteria for Geostatistical Realizations," *Natural Resources Research,* vol. 13, pp. 131-141, 2004.

[12] P. J. Smith, "A Recursive Formulation of the Old Problem of Obtaining Moments from Cumulants and Vice Versa," *The American Statistician,* vol. 49, pp. 217-218, 1995.

[13] C. Deutsch and A. Journel, *GSLIB: geostatistical software library and user's guide*, 2nd ed. New York: Oxford University Press, 1998.

[14] K. Jain and A. K. Nanda, "On multivariate weighted distributions," *Communications in Statistics - Theory and Methods,* vol. 24, pp. 2517-2539, 1995/01/01 1995.

[15] D. F. Machuca-Mory and C. V. Deutsch, "Locaton Dependent Variograms," in *Geostats 2008 - VIII International Geostatistics Congress*, Santiago, Chile, 2008, pp. 497-506.

[16] B. M. Sadler, G. B. Giannakis, and L. Keh-Shin, "Estimation and detection in non-Gaussian noise using higher order statistics," *Signal Processing, IEEE Transactions on*, vol. 42, pp. 2729-2741, 1994.

[17] S. Krishnan, "The Tau Model for Data Redundancy and Information Combination in Earth Sciences: Theory and Application," *Mathematical Geosciences*, vol. 40, pp. 705-727, 2008.